Numerical analysis study using Penzien model on dynamic response of pile foundation structures in a liquefied ground

Natsuki Adachi [1*], and *Tsuyoshi* Honda [1]

[1] Research & Development Institute, Takenaka Corporation, Japan

Abstract. This paper presents the results of dynamic centrifuge model tests conducted to verify the analysis program for seismic response evaluation of pile foundation structures. The model consisted of three layers: a liquefiable layer, a non-liquefiable layer, and a bearing stratum. In the numerical analysis, a Penzien-type lumped mass model was employed, which successfully reproduced the measured acceleration records. Subsequently, parametric studies were conducted on the seismic response of pile foundation structures using six actual buildings located in Nagoya and Osaka. The seismic responses were compared with and without liquefaction occurrence to investigate the effects of liquefaction on structural response. The results clarified that differences in soil stratigraphy significantly influence the dynamic response of superstructures.

1 Introduction

During the 1995 Kobe earthquake, it was reported that building damage on liquefied ground was less severe than that on non-liquefied ground [1]. This phenomenon is attributed to the so-called "liquefaction base-isolation effect", in which the reduction of ground stiffness due to liquefaction lengthens the natural period of the ground, thereby reducing seismic input to buildings. For structures on shallow foundations, the transmission path of seismic motion from the ground to buildings is relatively easy, making the mechanism of this liquefaction base-isolation effect comparatively clear. However, for pile foundation structures, the dynamic interaction of the pile-building-ground coupled system is complex.

Several researchers have conducted to investigate the behavior of pile foundation structures in liquefied ground using centrifuge model tests and numerical analyses [2-5]. In these previous studies, centrifuge experiments using simple single-layer or two-layer ground configurations have been conducted [2-4]. However, actual ground conditions comprise multiple layers of varying soil types, demonstrating more intricate stratification patterns. Although it would be desirable to experimentally examine all conceivable configurations of geological stratum compositions, such an approach is not practically feasible. Mori (2000) carried out numerical analyses reproducing the actual damage of pile foundation structures in liquefied layer [5]. However, systematic analyses of how the seismic response of structures with similar conditions changes when the geological stratum composition below the liquefied layer differs have not been conducted.

This study aims to investigate how pile foundation buildings in different regions respond differently to liquefaction versus non-liquefaction scenarios by conducting a parametric study using numerical analysis. For this purpose, seismic response analyses were performed on multiple existing building models in Nagoya and Osaka. The analysis program EENAPILE [8-10], which can account for liquefaction based on cumulative damage theory, was employed. This paper first presents a centrifuge model test and its numerical simulation to validate the analysis program, followed by a report on the parametric study results.

2 Centrifuge model test and numerical simulation of the test

2.1 Test model and material properties

The centrifuge model test was conducted in a centrifugal field of 50 G. Fig. 1 illustrates the centrifuge test model and the location of sensors. Tables 1 and 2 present the material properties of the ground, piles and structures. The ground model comprised three layers: a liquefiable layer at the top, a non-liquefiable layer beneath it, and a bearing stratum mixed with cement at the base. Both the liquefiable layer and non-liquefiable layer were formed using Iide Silica sand No. 6. Fig. 2 shows the grain size accumulation curve of Iide Silica sand No.6 [11]. The liquefiable layer was prepared using air-pluviation with the relative density (Dr) 70%, while the non-liquefiable layer was prepared using wet tamping with Dr 85%. Since this study focuses on the behavior of loose sand, the effect of grain size scaling is considered to be negligible. The groundwater level was set at GL-10mm in model scale. Two superstructure types were investigated: Model 1 consisted of five stainless steel plates with a thickness of 20 mm, while

* Corresponding author: adachi.natsuki@takenaka.co.jp

Model 2 comprised a 50 mm square aluminium tube with 2 mm wall thickness. Both models were connected to the pile heads via bolted joints. Both models were connected to the pile heads with bolt joints. The pile foundation consisted of four aluminium pipes with a diameter of 30 mm, with their tips embedded in the bearing stratum. The load per pile in the 50G field was approximately 10,000 kN for Model 1 and approximately 200 kN for Model 2. The acceleration wave in shown Fig. 3 was inputted from the base layer. This input motion was adjusted to a maximum acceleration of 350 Gal, which was derived from the ground surface acceleration recorded in Urayasu during the 2011 off the Pacific coast of Tohoku Earthquake using equivalent linear site response analysis.

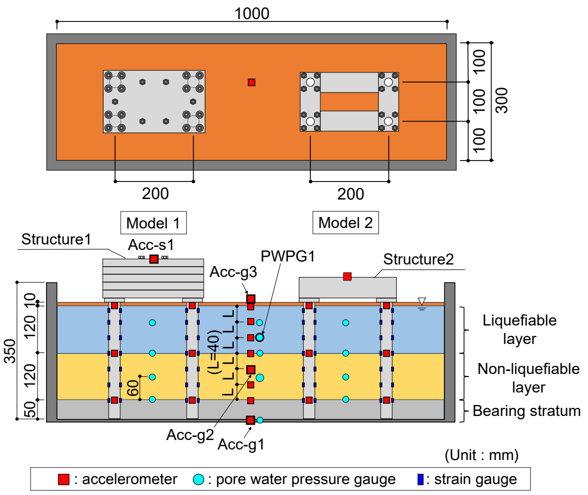

Fig. 1. Centrifuge test model and the location of sensors.

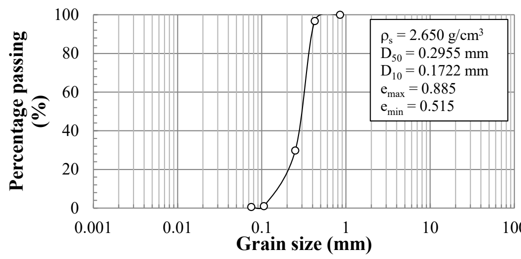

Fig. 2. Grain size accumulation curve of Iide Silica sand No. 6 [11].

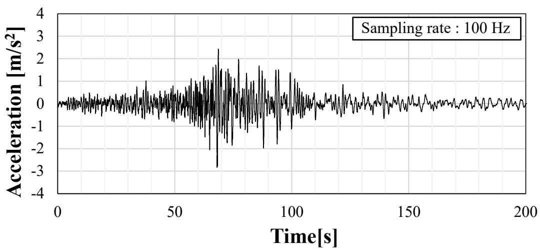

Fig. 3. Input motion used in the centrifuge model test.

2.2 Numerical simulation

2.2.1 Analysis program

In this study, numerical analyses were conducted using an analysis program (EENAPILE) capable of modeling liquefaction based on cumulative damage [8-10]. EENAPILE employs a Penzien-type lumped mass model to represent piles, superstructures, and the ground. The soil reaction springs surrounding the pile can account for the influence of the excess pore water pressure ratio, which is calculated from cumulative damage derived from ground shear stress and liquefaction strength curves, thereby enabling the modeling of liquefaction-induced effects on soil-pile interactions.

Table 1. Material properties of the ground in the test.

	Material	Preparation method
Liquefiable Layer	Iide Silica sand No. 6 (Dr = 70%, γ_w = 19.8kN/m^3)	Air-pluviation
Non-liquefiable layer	Iide Silica sand No. 6 (Dr = 85%, γ_w = 20.8kN/m^3)	Wet tamping
Bearing stratum	Iide Silica sand No.4 + Cement 100kg/m^3 (W/C = 100%)	Tamping

Table 2. Material properties of piles and structures in the test.

	Material	Size and Mass *1
Structure 1	Stainless steel plate	CS*2 = 260mm × 160mm t*3 =20 mm / 1 plate m*4 = 6.6kg / 1 plate
Structure 2	Square aluminum pipe	CS = 50mm × 50mm t =2 mm m = 0.6kg
Pile	Round aluminum pipe	D*5 = 30mm t = 3mm m = 0.2kg

Note : (*1) Values at 1G gravitation force field, (*2) CS : Cross section, (*3) t : Thickness, (*4) m : Mass, (*5) D : Diameter

2.2.2 Analysis model and parameters

An overview of the analytical model is presented in Fig. 4. Penzien-type lumped mass model was employed to represent the pile, superstructure, and ground. The structural mass point was positioned at the center of gravity of the structure. Material constants for the pile and structure are summarized in Table 3. Physical properties corresponding to a centrifugal field of 50 G were adopted for the pile and superstructure. It should be noted that the pile was modeled as a solid cross-section in the analysis, whereas a hollow aluminum pipe was used in the centrifuge model test. To maintain equivalent mass, the density of the pile was adjusted in the analysis. Although two structural models were investigated in the experiments, only the simulation results for Model 1 are presented in this paper. The initial shear stiffness of the ground was determined from the density of each layer and the shear wave velocity illustrated in Fig. 5. Liquefaction strength curves for the liquefiable and non-liquefiable layers employed in the analysis are shown in Fig. 6. These curves were based on values for Iide Silica Sand No. 6 derived by the methodology proposed by Honda et al. [11]. For the liquefiable layer, the liquefaction strength curve obtained from specimens prepared by air-pluviation with Dr 70% was adopted. In contrast, for the non-liquefiable layer, the curve from specimens prepared by wet tamping with Dr 85% was utilized. The hyperbolic model was applied to characterize the dynamic deformation behavior of liquefiable layer. Dynamic properties of the surface backfill soil and non-liquefiable layer were obtained from the characteristics presented in Fig. 7 [12]. Ground material parameters are summarized in Table 4. The internal friction angle was determined from cyclic triaxial test results obtained from specimens with Dr 70% and Dr 85%, both of which yielded an internal friction angle of 38 degrees.

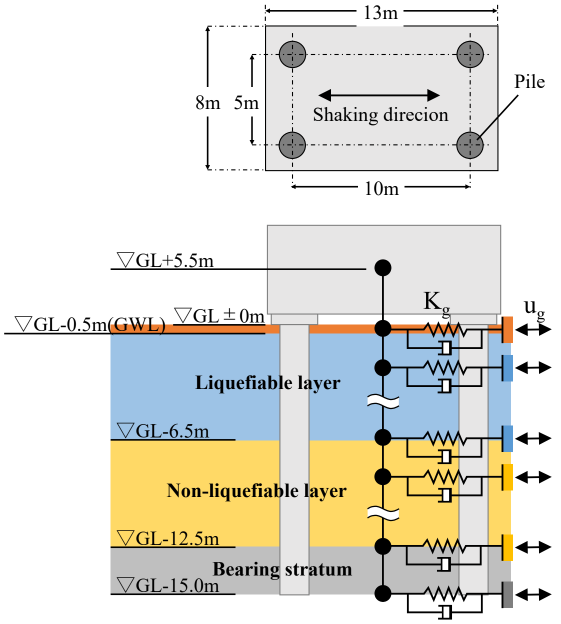

Fig. 4. Penzien-type lumped mass model in the numerical simulation.

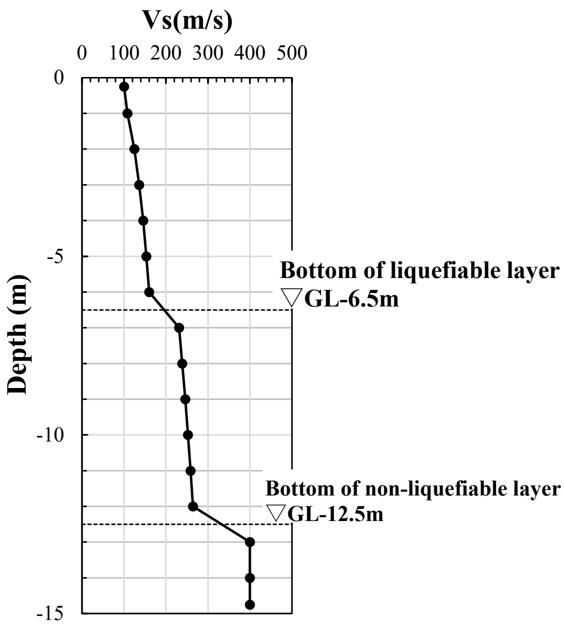

Fig. 5. Shear wave velocity of the ground used in the numerical simulation.

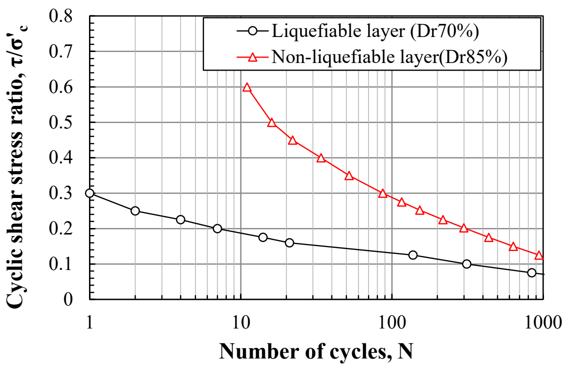

Fig. 6. Liquefaction strength curves used in the numerical simulation [11].

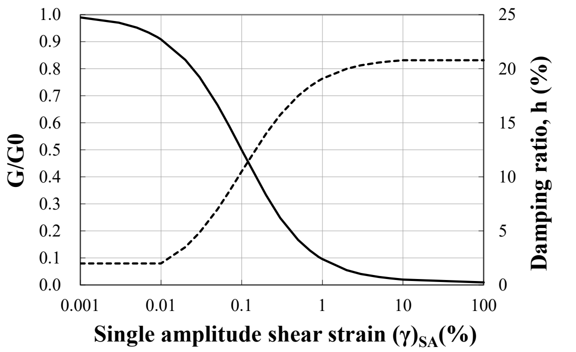

Fig. 7. Dynamic properties of the surface backfill soil and the non-liquefiable layer used in the numerical simulation [12].

Table 3. Properties of the structure and the pile used in the numerical simulation.

Structure 1	Weight :	40411kN
	Area :	13m × 8m
	Damping ratio :	2%
Pile	Number of piles :	4 piles
	Diameter :	1.5m
	Length :	15m
	Area :	0.636m^2
	Young's modulus :	6.83×10^{7}kN/m^2
	Second moment of area :	0.147m^4
	Unit weight :	9.39kN/m^3
	Damping ratio :	2%

Table 4. Properties of the ground used in the numerical simulation.

G.L. (m)	Layer	Thickness(m)	γ (kN/m^3)	h (%)	φ (°)
0 ~ -0.5	Backfill soil	0.5	16.0	2	38
-0.5~ -6.5	Liquefiable layer	6.0	19.8	2	38
-6.5~ -12.5	Non-liquefiable layer	6.0	20.1	2	38
-12.5~ -15.0	Bearing stratum (elastic)	2.5	20.2	2	-

2.3 Test and simulation result

Fig. 8 shows the time histories of excess pore water pressure ratios in the liquefiable layer obtained from both the centrifuge model test and the numerical analysis. In the test, the maximum excess pore water pressure ratio reached 1.0, and the liquefied state persisted from 70 to 150 seconds. The difference in the

 https://doi.org/10.1051/e3sconf/202673003016

accumulation of excess pore water pressure between the test and analysis is explained as follows. In the test, the initial shear history is considered to strengthen soil particle interlocking, which is considered to increase the liquefaction strength and delay the accumulation of excess pore water pressure. In contrast, such effects are not reflected in the analysis, resulting in a more rapid increase in excess pore water pressure.

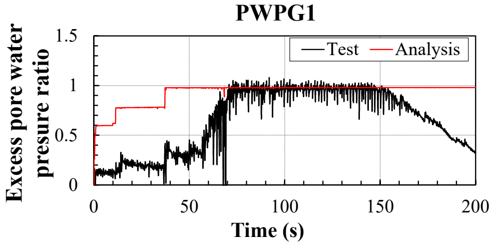

Fig. 8. Time histories of excess pore water pressure ratios in the test and the analysis.

Figs.9a and 9b present the acceleration time histories of the ground and superstructure obtained from the experiment. Notably, cyclic mobility was observed in the liquefiable layer (Acc-g3) after 70 seconds, when the excess pore water pressure ratio increased to approximately 1.0. In Figs.9a and 9b, the experimental results are shown as a black line and the analytical results are shown as a red line for comparison. Comparison of the two results confirmed that the acceleration wave form and phase characteristics of the superstructure were nearly identical, indicating that the numerical analysis model successfully reproduced the phenomena observed in the experiment. However, a notable discrepancy was observed at Acc-g3. This is attributed to differences in soil deformation mechanisms. In the centrifuge model test, the soil undergoes volumetric changes and free surface effects in addition to cyclic mobility. In contrast, the one-dimensional columnar model constrains volumetric changes, resulting in acceleration from cyclic mobility only. Furthermore, Fig. 9(c) presents a comparison of the acceleration response spectrum between the experimental and analytical results. The response spectrum calculated from the analytical results showed a predominant period of 1.08 seconds, which was nearly identical to the experimental results, although the maximum values differed. Based on these results, it was confirmed that EENAPILE can reproduce the seismic response of pile-supported buildings on liquefied ground.

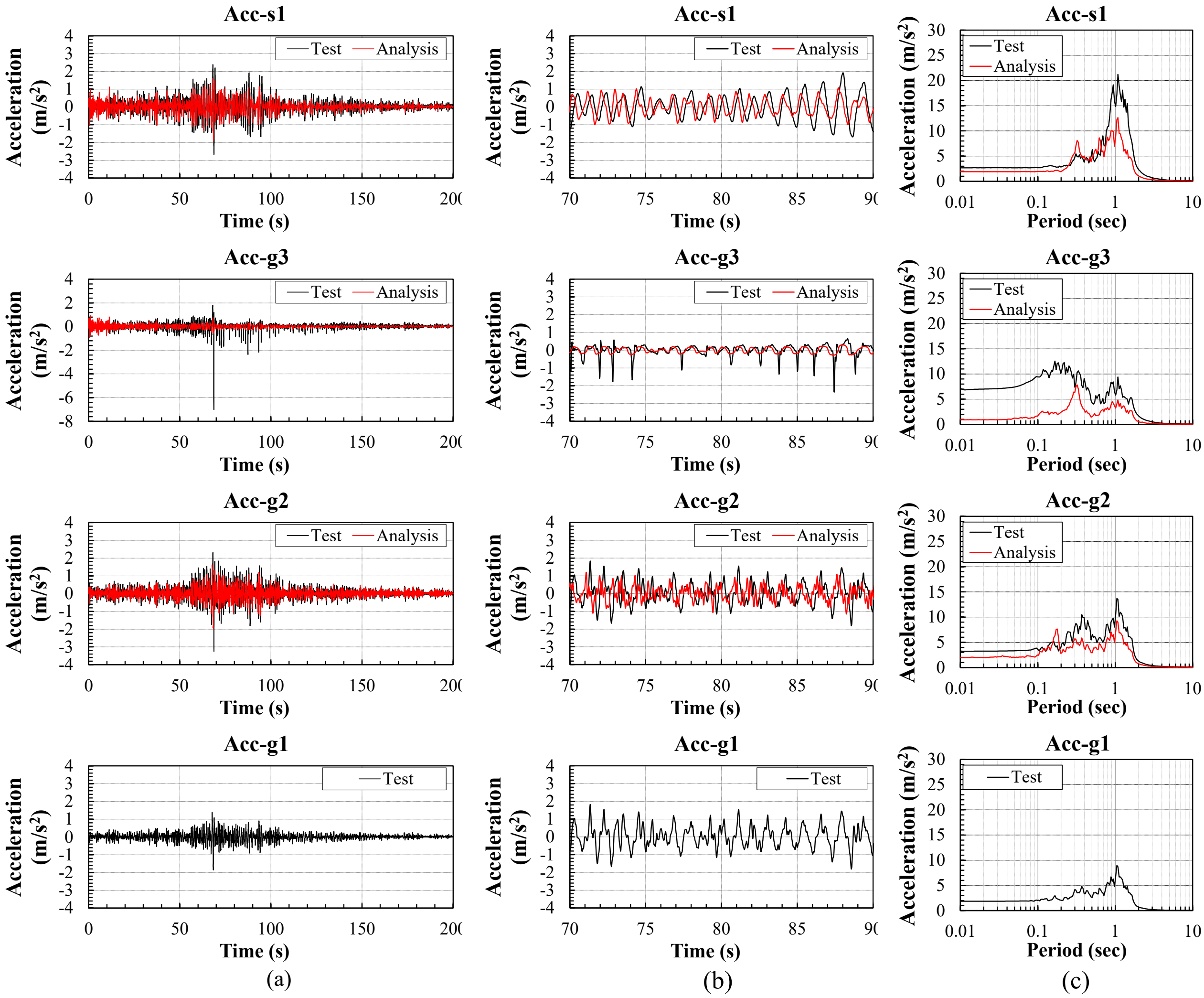

Fig. 9. Results in the test and the analysis: (a) acceleration, (b) accelerations (70-90s) and (c) acceleration response spectrum.

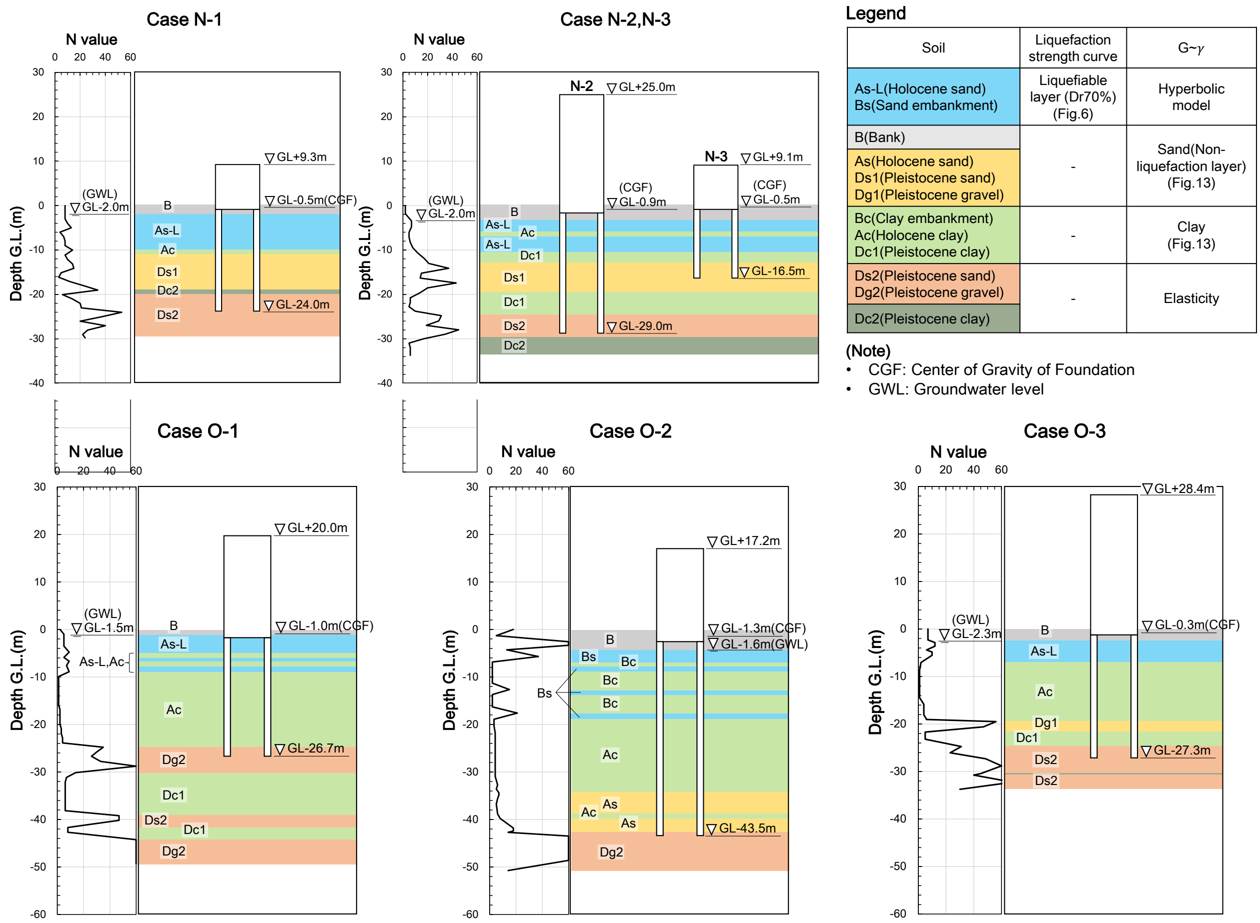

Fig. 10. Geological stratum compositions in each case.

3 Parametric study using Penzien model

3.1 Objective of parametric study

Geological stratum compositions exhibit regional characteristics that depend on the geological history and depositional environment of each area. To investigate how such regional differences affect the seismic response of pile-supported buildings on liquefiable ground, a parametric study using numerical analysis was conducted. Seismic response analyses using the Penzien model were performed for actual buildings in Nagoya and Osaka, two representative cities in Japan with distinct geological characteristics. The effects of liquefaction on building response were compared between regions to examine differences in response characteristics due to variations in geological stratum composition. The geological characteristics of each region are described below.

The geological stratum composition in the Nagoya City area consists of the Yadagawa Formation of the Tokai Group as the base layer, overlain by the Ama-Yatomi Formation and the Atsuta Formation. These layers are classified as Pleistocene deposits. The uppermost layers are composed of Holocene deposits (Nanyo Formation) and fill material. The Holocene deposits began to accumulate approximately 10,000 years ago with a rise in sea level, during which marine clay filled the valleys. Subsequently, deltaic and floodplain deposits of rivers, primarily composed of sand, advanced downstream and covered the marine

Table 5. Properties of buildings and piles in seismic response analyses.

Area	Case	Building	Pile
Nagoya	N-1	SS[*1] : S L_x[*2]=30m,L_y[*3]=81m H[*4]=9.3m T_1[*5]=0.28s	SC Pile[*6] D[*7]=400mm N[*8]=108
	N-2	SS : S L_x=15.9m, L_y=36m H=25m T_1=0.75s	SC Pile D=900mm N=21
	N-3	SS : S L_x=14.7m, L_y=28m H=9.1m T_1=0.27s	SC Pile D=500mm N=15
Osaka	O-1	SS : RC L_x=17.5m, L_y=28.8m H=20.0m T_1=0.34s	CIP Pile[*9] D=1600mm N=15
	O-2	SS : S L_x=32.4m,L_y=120.9m H=17.2m T_1=0.52s	SC Pile D=800mm N=48
	O-3	SS : S, SRC L_x=73m, L_y=153.7m H=28.4m T_1=0.86s	SC Pile D=800mm N=120

layers, while clay accumulated in back marshes distant from the river channels. The Holocene deposits and embankment layers form soft ground because these layers have been deposited recently and have not experienced loads exceeding the current overburden pressure. [6] The geological stratum composition of the Osaka Plain consists, from top to bottom, of Holocene deposits, upper Pleistocene layers, and the Osaka Group. The Holocene deposits comprise alternating layers of sandy soil and clay. In areas near rivers, the Holocene sandy soil layers are often assessed as having high liquefaction potential. The Ma13 layer, a soft marine clay deposited in the lower part of the Holocene deposits, is very thick and exists in a nearly normally consolidated state. The upper Pleistocene layer comprises alternate layers of gravel and clay. The Pleistocene Gravel Layer (Dg1), deposited below the Ma13 layer, exhibits very high N-values and serves as a strong bearing stratum for pile-supported structures. The upper Pleistocene clay layer (Ma12) is deposited beneath the Dg1 layer. [7]

3.2 Analysis conditions

In this study, a total of six existing buildings were selected for analysis, three each from Nagoya City and Osaka City. The selected buildings ranged from 2 to 7 stories with either steel (S) or reinforced concrete (RC) structural systems, all supported by pile foundations. Detailed information on building dimensions and pile specifications is presented in Table 5. Cases N-2 and N-3 are buildings located on the same site.

Each building was analyzed under two conditions: the first case included liquefaction effects, while the second case excluded them. The building responses in both cases were compared. The shear stiffness of the buildings was determined based on the structural models established at the design stage. Fig. 10 presents the N-value depth profiles and geological stratum compositions for each case. The geological stratum composition was established from soil investigation results obtained at each site. The initial shear stiffness of each stratum was calculated from shear wave velocities derived from N-values according to the following formula proposed by Imai [13].

$$\text{Holocene soil (As)}: V_s = 80.6N^{0.331} \tag{1}$$

$$\text{Holocene clay (Ac)}: V_s = 102N^{0.292} \tag{2}$$

$$\text{Pleistocene soil (Ds)}: V_s = 97.2N^{0.323} \tag{3}$$

$$\text{Pleistocene clay (Dc)}: V_s = 114N^{0.292} \tag{4}$$

For the dynamic deformation properties of liquefiable layers, the liquefaction strength curve illustrated in Fig. 6 and the hyperbolic model were used. In cases without liquefaction, stiffness degradation due to excess pore water pressure was not considered. For non-liquefiable sandy and clayey soil layers, the dynamic properties presented in Fig.11 were applied. Stiffness degradation due to excess pore water pressure was not incorporated for these layers in any of the analysis cases. The input motion for all analysis cases was represented by the seismic wave shown in Fig. 12. It was derived based on the standard acceleration response spectrum specified in the Japanese Building Code and was created using the Hachinohe phase characteristics.

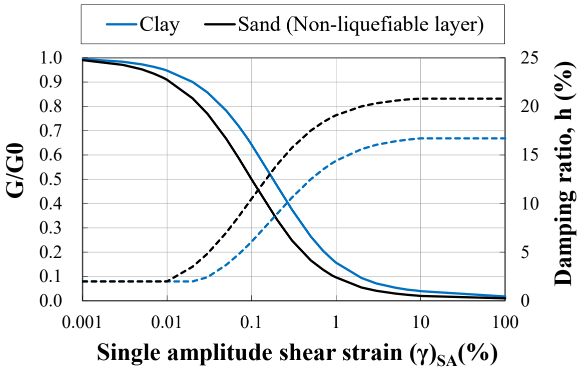

Fig. 11. Dynamic properties of the non-liquefiable layer and clay used in seismic response analyses[12].

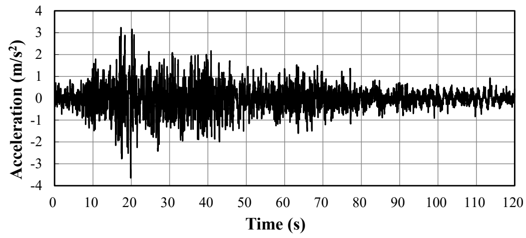

Fig. 12. Input motion used in seismic response analyses.

3.3 Results and Discussion

For each analysis case, the results were compared between cases with and without liquefaction. Fig.13 presents radar charts showing the maximum acceleration, velocity, and displacement at the building top and foundation, along with the maximum bending moment and shear force in the piles. Red and black lines represent cases with and without liquefaction consideration, respectively. Based on the maximum acceleration and velocity at the building top, the results were categorized into two groups. The three Nagoya cases exhibited significant response reduction when liquefaction was considered. In contrast, the three Osaka cases showed minimal response variation regardless of liquefaction. Table 6 presents the eigenvalue analysis results. The natural period of the ground (T_G) was calculated from initial shear wave velocity. The natural period of the building (T_B) represents values calculated assuming fixed-base conditions. The ground natural period in Nagoya ranged from approximately 0.5 to 0.6 seconds, while that in Osaka ranged from approximately 0.8 to 1.1 seconds. Due to the presence of thick, soft clay layers, the Osaka ground is considered to have vibration characteristics that amplify long-period components. As a result, it is inferred that the building responses in the Osaka cases remained nearly equivalent regardless of liquefaction consideration.

(Legend) —□—: Case of consideration without liquefaction —●—: Case of consideration with liquefaction

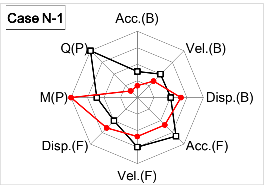

			Analysis result (Max)	
Consideration of liquefaction			Without	With
Building top	Acc.(B)	Accelation (m/s^2)	9.33	4.37
	Vel.(B)	Velocity (m/s)	0.59	0.39
	Disp.(B)	Displacement (m)	0.30	0.28
Foundation	Acc.(F)	Accelation (m/s^2)	2.90	1.36
	Vel.(F)	Velocity (m/s)	0.38	0.31
	Disp.(F)	Displacement (m)	0.29	0.28
Pile top	M(P)	Bending moment (kNm)	46	203
	Q(P)	Shear force (kN)	48	29

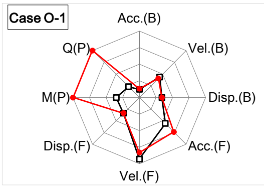

			Analysis result (Max)	
Consideration of liquefaction			Without	With
Building top	Acc.(B)	Accelation (m/s^2)	2.40	2.60
	Vel.(B)	Velocity (m/s)	0.61	0.57
	Disp.(B)	Displacement (m)	0.20	0.20
Foundation	Acc.(F)	Accelation (m/s^2)	1.67	2.20
	Vel.(F)	Velocity (m/s)	0.56	0.50
	Disp.(F)	Displacement (m)	0.20	0.20
Pile top	M(P)	Bending moment (kNm)	8114	23324
	Q(P)	Shear force (kN)	466	2044

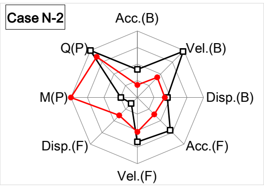

			Analysis result (Max)	
Consideration of liquefaction			Without	With
Building top	Acc.(B)	Accelation (m/s^2)	8.42	3.74
	Vel.(B)	Velocity (m/s)	1.37	0.60
	Disp.(B)	Displacement (m)	0.27	0.25
Foundation	Acc.(F)	Accelation (m/s^2)	2.11	1.10
	Vel.(F)	Velocity (m/s)	0.40	0.31
	Disp.(F)	Displacement (m)	0.08	0.23
Pile top	M(P)	Bending moment (kNm)	1745	7042
	Q(P)	Shear force (kN)	676	585

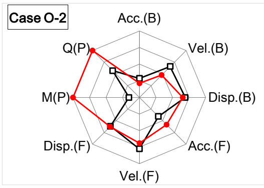

			Analysis result (Max)	
Consideration of liquefaction			Without	With
Building top	Acc.(B)	Accelation (m/s^2)	5.72	4.23
	Vel.(B)	Velocity (m/s)	0.92	0.67
	Disp.(B)	Displacement (m)	0.42	0.39
Foundation	Acc.(F)	Accelation (m/s^2)	1.22	1.75
	Vel.(F)	Velocity (m/s)	0.47	0.41
	Disp.(F)	Displacement (m)	0.37	0.37
Pile top	M(P)	Bending moment (kNm)	1083	7001
	Q(P)	Shear force (kN)	572	1007

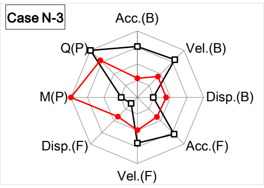

			Analysis result (Max)	
Consideration of liquefaction			Without	With
Building top	Acc.(B)	Accelation (m/s^2)	15.29	5.73
	Vel.(B)	Velocity (m/s)	1.12	0.62
	Disp.(B)	Displacement (m)	0.15	0.26
Foundation	Acc.(F)	Accelation (m/s^2)	2.36	1.26
	Vel.(F)	Velocity (m/s)	0.41	0.30
	Disp.(F)	Displacement (m)	0.08	0.25
Pile top	M(P)	Bending moment (kNm)	321	1331
	Q(P)	Shear force (kN)	239	188

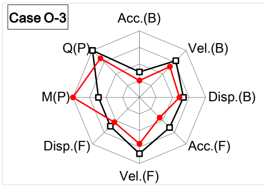

			Analysis result (Max)	
Consideration of liquefaction			Without	With
Building top	Acc.(B)	Accelation (m/s^2)	7.64	5.08
	Vel.(B)	Velocity (m/s)	1.09	0.91
	Disp.(B)	Displacement (m)	0.40	0.36
Foundation	Acc.(F)	Accelation (m/s^2)	1.94	1.29
	Vel.(F)	Velocity (m/s)	0.51	0.42
	Disp.(F)	Displacement (m)	0.37	0.32
Pile top	M(P)	Bending moment (kNm)	17677	28645
	Q(P)	Shear force (kN)	4083	3387

Fig. 13. Comparison of analysis results between liquefaction and non-liquefaction cases.

Table 6. Natural periods of buildings and grounds obtained from eigenvalue analysis.

Case	T_B (s)	T_G (s)
N-1	0.28	0.53
N-2	0.75	0.61
N-3	0.27	0.61
O-1	0.34	1.10
O-2	0.52	1.16
O-3	0.86	0.78

To examine this difference, time history responses for representative cases N-1 and O-1 are presented in Figs.14 and 15, respectively. Figs.14a and 15a present the time histories of excess pore water pressure ratio for the analysis cases with liquefaction consideration. Figs. 14c and 15c show the Fourier spectra calculated from the acceleration waveforms between 20 and 120 seconds, respectively. In both cases with liquefaction, excess pore water pressure ratios reached 1.0 and the ground was liquefied during this time period. For case N-1, acceleration responses at the building top were comparable until 10 seconds, regard-less of liquefaction consideration. During the liquefaction development phase from 10 to 20 seconds, the acceleration was substantially reduced in the liquefaction case. This reduction persisted beyond 20 seconds under complete liquefaction. The acceleration at the foundation also showed lower values when liquefaction was considered. For case O-1, the acceleration in the liquefiable layer decreased upon reaching complete liquefaction. Nevertheless, acceleration responses at both the foundation and building top remained nearly identical regardless of liquefaction consideration.

Focusing on the Fourier spectra of the liquefiable layer, distinct differences were observed between the two cases. In case N-1, short-period components close to the natural period of the building were predominant in the non-liquefaction condition. However, in case O-1, the magnitude of short-period components close to the building's natural period was comparable regardless of whether liquefaction occurred. It is inferred that the ground in case O-1 has vibration characteristics that do

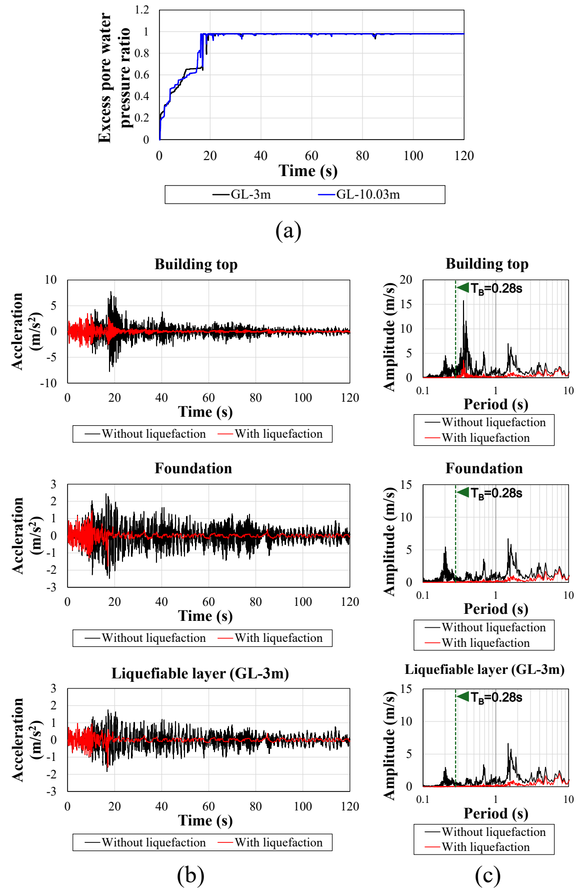

Fig. 14. Result of Case N-1 : (a) excess pore water pressure ratio, (b) acceleration and (c) Fourier spectrum (20-120s).

not significantly amplify short-period components, and therefore the effect of ground period lengthening due to liquefaction is limited. This point requires further investigation in future studies.

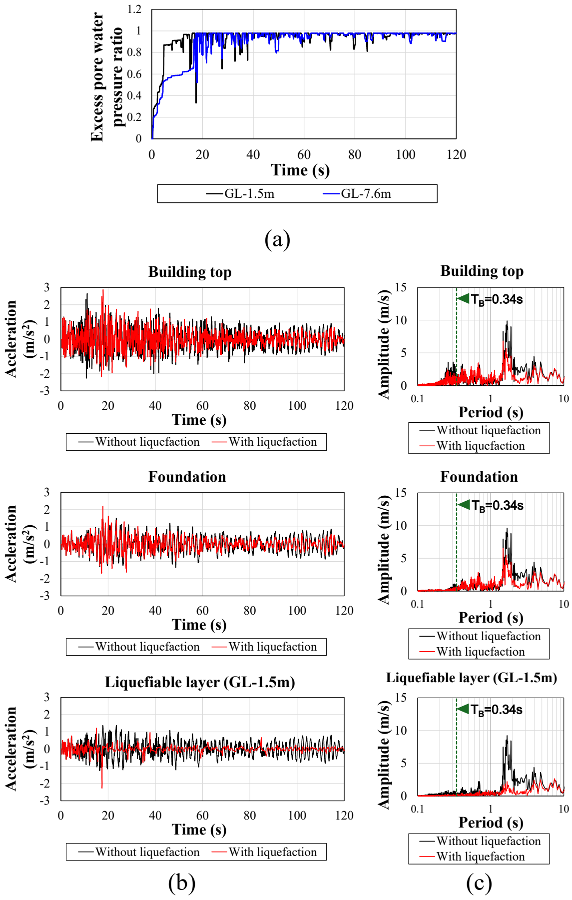

Fig. 15. Result of Case O-1: (a) excess pore water pressure ratio, (b) acceleration and (c) Fourier spectrum (20-120s).

4 Summary

This study presents the results of centrifuge model tests and numerical simulations using a Penzien-type lumped mass model, and the parametric studies on actual buildings in Nagoya and Osaka. The main findings are summarized as follows :

1) The centrifuge model test was performed and the numerical simulation was conducted using the Penzien-type lumped mass model. The validity of the analysis tool was evaluated through the results.
2) A parametric study was conducted to investigate the dynamic response characteristics of pile-supported structures in liquefied ground using the Penzien model. Six actual buildings were analyzed, three each from Nagoya and Osaka, representing different geological conditions in Japan.
3) All three cases in Nagoya exhibited substantial response reduction when liquefaction was considered, with notable decreases in maximum acceleration and velocity at the building top. In contrast, all three cases in Osaka showed minimal response variation regardless of liquefaction consideration.
4) Ground natural periods in the analysed cases in Nagoya ranged from 0.5 to 0.6 seconds, while those in Osaka ranged from 0.8 to 1.1 seconds due to thick, soft clay layers. It is inferred that when the ground exhibits a relatively long natural period, the base-isolation effect associated with period lengthening due to liquefaction may be limited. However, this point requires detailed investigation in future studies.

References

1. Earthquake Engineering Committee, Japan Society of Civil Engineers and Soil Liquefaction under Level II Earthquake Motion Subcommittee, Soil liquefaction under Level II earthquake motion, JSCE, 89-155 (2003)
2. Y. Miyamoto, A. Fukuoka, N. Adachi and K. Koyamada, Pile response induced by inertial and kinematic interaction in liquefied soil deposit centrifuge model test for pile foundation in saturated sand layers and its analytical study, J. Struct. Constr. Eng., AIJ, 494, 51-58 (1997) https://doi.org/10.3130/aijs.62.51_1
3. H. Mano and Y. Shamoto, Influence of soil liquefaction beneath foundations on seismic earth pressures acting on embedments based on centrifuge tests, J. Struct. Constr. Eng., AIJ, **74**, 2045-2051 (2009) https://doi.org/10.3130/aijs.60.41_1
4. K. Tokimatsu, H. Suzuki and M. Sato, Effects of dynamic soil-pile-structure interaction on pile stress, J. Struct. Constr. Eng., AIJ, **587**, 125-132 (2005) https://doi.org/10.3130/aijs.70.125_1
5. S. Mori, Proposal of a spring-mass model for structures on pile foundations and its application to damaged structures, J. Appl. Mech., JSCE, **3**, 609-620 (2000) https://doi.org/10.2208/journalam.3.609
6. Chubu Branch of JGS, Geotechnical data of subsoils in Nagoya (New edition, 1988), Nagoya Ground Map Publishing Committee (1998)
7. Kansai Branch of JGS and KAGI, The ground of Osaka, Corona Publishing Co., Ltd. (1987)
8. A. Imamura, F. Yagishita, H. Yoshida, T. Shiomi and K. Tokimatsu, the construction of beam-on-spring model considered liquefaction between the piles Part 1. A summary of suggested model, Summ. Tech. Pap. Annu. Meet., AIJ, 2003, 359-360 (2003)
9. T. Namikawa, A. Imamura, F. Yagishita, T. Shiomi, R. Babasaki and K. Tokimatsu, The construction of beam-on-spring model considered liquefaction between the piles Part 2. Seismic behavior of group pile model in centrifuge test, Summ. Tech. Pap. Annu. Meet., AIJ, 2003, 361-362 (2003)
10. A. Imamura, H. Yoshida, F. Yagishita, T. Shiomi and K. Tokimatsu, The construction of beam-on-spring model considered liquefaction between the piles Part 3. Simulation of dynamic centrifuge test, Summ. Tech. Pap. Annu. Meet., AIJ, 2003, 363-364 (2003)
11. T. Honda, T. Kiyota, C. Wu and Y. Shigeno, Evaluation of liquefaction strength curve using cumulative dissipated energy, Jpn. Geotech. J., **15**, 213-224 (2020) https://doi.org/10.3208/jgs.15.213
12. Seismic response analysis and design of buildings considering dynamic soil-structure interaction, AIJ, **55** (2006)
13. T. Imai, P- and S-wave velocities of the ground in Japan, Proc. 9th Int. Conf. Soil Mech. Found. Eng., 2, 257-260 (1977)